JOURNAL OF AIRCRAFT
Vol. 31, No. 2, March–April 1994

Modal Coordinates for Aeroelastic Analysis with Large Local Structural Variations

M. Karpel*
Technion—Israel Institute of Technology, Haifa, Israel
and
C. D. Wieseman†
NASA Langley Research Center, Hampton, Virginia 23681

Time domain aeroelastic equations of motion are formulated in a way that allows large local structural variations with a state-space model that is based on a relatively small number of generalized coordinates. Free-free or restrained vibration modes are first calculated for a nominal finite element model loaded with relatively large fictitious masses located at the area of structural variations. These modes and the associated oscillatory aerodynamic force coefficient matrices are used to construct a time-domain model for a basic aeroelastic case where the fictitious mass contribution to the generalized mass matrix is removed. High-accuracy aeroelastic investigations of the effects of structural variations can then be performed by simply introducing mass, stiffness, and damping coupling terms. It is shown that the number of modes required for the investigation of large stiffness variations is substantially lower than that required when fictitious masses are not used, and only slightly larger than the number of modes required for direct aeroelastic analysis of a single structural case.

Nomenclature

$[A_1]$, $[A_2]$ = matrix coefficients of the aerodynamic approximation, Eq. (13)
b = reference semichord
$[D]$, $[E]$ = matrix coefficients of the aerodynamic approximation, Eq. (13)
$[GB]$ = generalized damping matrix
$[GK]$ = generalized stiffness matrix
$[GM]$ = generalized mass matrix
g = structural damping
$[I]$ = identity matrix
$[K]$ = stiffness matrix of the nominal structure
k = reduced frequency, $\omega b/V$
k_θ = pitch stiffness of wing-store connection
$[M]$ = mass matrix of the nominal structure
$[M_c]$ = control mass-coupling matrix, Eq. (7)
$[M_f]$ = matrix of fictitious masses added to the nominal structure
m = number of aerodynamic roots
n = number of degrees of freedom in the finite element model
n_c = number of control surfaces
n_f = number of modes with fictitious masses taken into account for aeroelastic modeling
n_g = number of gust velocity modes
$[Q(ik)]$ = generalized aerodynamic force coefficient matrix
$[\tilde{Q}_b(\bar{s})]$ = approximated generalized aerodynamic force matrix, Eq. (13)
q = dynamic pressure
$[R]$ = a diagonal aerodynamic lag matrix, Eq. (13)
s = Laplace variable
$\bar{s}$ = nondimensional Laplace variable, sb/V
V = true airspeed
$\boldsymbol{x}$ = discrete structural displacement vector
$\boldsymbol{x}_a$ = aerodynamic state vector, Eq. (14)
$[\Delta K]$ = changes in stiffness matrix
$[\Delta M]$ = changes in mass matrix
$[\zeta]$ = modal damping coefficient matrix
ξ = generalized displacements, Eq. (14)
$[\phi]$ = matrix of vibration modes in discrete coordinates
$[\chi]$ = undamped eigenvectors in modal coordinates
ω = vibration frequency
$[\omega]$ = diagonal matrix of natural frequencies

Subscripts
a = actual case of stiffness variation
b = basic structure modes
ba = structural variation—basic to actual
c = control surface deflection modes
d = physical weighting design conditions
F = at flutter
f = associated with fictitious masses
g = gust velocity modes

Introduction

THE evaluation of the effects of structural property variations on flutter and aeroelastic response has an important role in the design of flight vehicles. Investigations in which such evaluations are required are structural optimization, parametric studies, damage effects, and structural changes during dynamic response. Common aeroelastic analyses start with the calculation of a limited set of low-frequency normal modes which serve as generalized coordinates.[1] Repeated calculation of the normal modes and the associated generalized aerodynamic force coefficients every time a structural property changes is often impractical. An additional problem is how to deal with the changing coordinates during time-domain

Presented as Paper 91-102 at the DGLR/AAAF/RAeS/AIAA International Forum on Aeroelasticity and Structural Dynamics, Aachen, Germany, June 3–6, 1991; received Sept. 25, 1991; revision received Nov. 2, 1992; accepted for publication Nov. 5, 1992.

*Associate Professor, Faculty of Aerospace Engineering. Member AIAA.

†Aerospace Engineer, Aeroelastic Analysis and Optimization Branch, M/S 246. Member AIAA.

response analysis. These problems can be resolved by performing the entire analysis with a constant set of modal coordinates.

Various applications, like the structural optimization of Ref. 2 and the damage effects on flutter of Ref. 3, used the vibration modes of a basic structure as generalized coordinates and accounted for structural changes by introducing stiffness, mass, and damping coupling terms. The basic assumption is that after the structural modifications, the structural displacements may still be assumed to be a linear combination of the original modes. This approach is limited to moderate structural changes and may require a relatively large number of modes in order to achieve a reasonable level of accuracy. Reference 3 indicated unacceptable flutter errors when large local damage effects were analyzed using fixed modes.

A modified approach is taken in this article for cases with large structural variations at a few a priori known locations. The idea is that the effects of large structural variations can be properly accounted for only when the modes which serve as generalized coordinates contain significant distortions in the vicinity of the varying structural elements. This is achieved by calculating a set of normal modes for a nominal structure loaded with additional relatively large fictitious masses at grid points to which the varying elements are connected. The presence of fictitious masses force the normal modes to contain local distortions that cause internal stresses which balance the inertial forces associated with the fictitious masses. The fictitious-mass concept was first introduced in the context of substructure modal coupling by Karpel and Newman.[4] It was used by Karpel[5] for efficient vibration modes analysis of aircraft with multiple external store configurations, and by Livne[6] in reduced-order eigenvalue sensitivities of control augmented structures. All these applications yielded very efficient, easy-to-apply computational schemes.

The time-domain, state-space, constant coefficient aeroelastic equations of motion in this work are based on the minimum-state (MS) modeling method.[7,8] The MS rational approximations of the unsteady aerodynamic force coefficient matrices are performed with physical weighting of the oscillatory aerodynamic data,[8] which has been demonstrated[2,9,10] to yield lower-order models than those of other modeling methods. The modeling formulation is modified to accommodate the fictitious mass modes in a way that allows efficient, high-accuracy investigations of the effects of large local structural variations on aeroelastic and aeroservoelastic phenomena.

Normal Modes

The free air-off matrix equation of motion of an n degrees-of-freedom nominal undamped structure loaded with fictitious masses is

$$[M + M_f]\{\ddot{x}\} + [K]\{x\} = \{0\} \tag{1}$$

where the elements of the fictitious mass matrix $[M_f]$ are zero, except for the terms added to the structure at the locations of subsequent large structural variations. Standard normal modes analysis codes (such as NASTRAN) can solve Eq. (1) for a set of n_f low-frequency fictitious mass modes $[\phi_f]$ where $n_f << n$, which forms the basis for the generalized structural coordinates in subsequent aeroelastic analyses. The diagonal generalized mass and stiffness matrices associated with $[\phi_f]$ satisfy

$$[GM_f] = [\phi_f]^T[M + M_f][\phi_f] \tag{2}$$

$$[GK_f] = [\phi_f]^T[K][\phi_f] = [\omega_f]^2[GM_f] \tag{3}$$

where $[\omega_f]$ is a diagonal matrix of the natural frequencies, including zero frequencies for rigid-body modes. The free undamped equation of motion of an actual structure whose mass and stiffness matrices differ from those of the nominal structure by $[\Delta M]$ and $[\Delta K]$ is

$$[M + \Delta M]\{\ddot{x}\} + [K + \Delta K]\{x\} = \{0\} \tag{4}$$

It is assumed that the displacement vector $\{x\}$ of Eq. (4) is a linear combination of the fictitious-mass modes, namely

$$\{x\} = [\phi_f]\{\xi_f\} \tag{5}$$

Substitution of Eq. (5) in Eq. (4), and premultiplication by $[\phi_f]^T$ yield, by way of Eqs. (2) and (3)

$$([GM_f] - [\phi_f]^T[M_f - \Delta M][\phi_f])\{\ddot{\xi}_f\} + ([GK_f] + [\phi_f]^T[\Delta K][\phi_f])\{\xi_f\} = \{0\} \tag{6}$$

which yields an $n_f \times n_f$ eigenvalue problem that can be solved for the natural frequencies, $[\omega_a]$, of the actual structure (without fictitious masses). The accuracy of the resulting frequency values, when compared to those obtained directly from the finite element model, is a function of the magnitudes of $[M_f]$, $[\Delta M]$, and $[\Delta K]$. Simple guidelines for an adequate choice of the values of $[M_f]$ are given, demonstrated, and discussed in the numerical example section.

The fictitious masses needed to facilitate wide ranges of stiffness and mass variations are usually significantly larger than the nominal masses attached to the fictitious mass points. While the added fictitious masses must have positive values [otherwise the mass matrix in Eq. (1) would not be positive semidefinite], the structural variations in $[\Delta M]$ and $[\Delta K]$ may have either positive or negative values.

Aeroelastic Modeling

Basic System

The fictitious mass modes $[\phi_f]$ resulting from Eq. (1), and the kinematically defined control surface deflection and gust velocity modes, $[\phi_c]$ and $[\phi_g(ik)]$, are used to generate the associated $n_f \times n_f$, $n_f \times n_c$ and $n_f \times n_g$ generalized oscillatory aerodynamic force (GAF) matrices, $[Q_{fb}(ik)]$, $[Q_{fc}(ik)]$ and $[Q_{fg}(ik)]$, at various tabulated reduced frequency (k) values. Standard codes, like those which utilize the doublet-lattice method,[11] are commercially available for this purpose. The finite element code that calculates $[\phi_f]$ can also be used[2] to calculate the control mass-coupling matrix

$$[M_{cf}] = [\phi_f]^T[M][\phi_c] \tag{7}$$

The fictitious mass modes can serve as a constant set of generalized coordinates for a wide range of additive and subtractive structural variations in the vicinity of the fictitious masses. It is more convenient, however, to first transform $[\phi_f]$ to a set of modes associated with a basic structural configuration which has no fictitious masses. One of the structural variations to be analyzed is chosen to form the "basic" aeroelastic system. In addition to the $[M_f]$ difference, the mass and stiffness matrices of this case may be different from those of the fictitious mass case by $[\Delta M_b]$ and $[\Delta K_b]$. Other structural variations will be referred to as "actual" cases. The eigensolution resulting from Eq. (6) with $[\Delta M]$ and $[\Delta K]$ replaced by $[\Delta M_b]$ and $[\Delta K_b]$ yields n_f natural frequencies, $[\omega_b]$, and the associated square eigenvector matrix $[\chi_b]$. The eigenvectors are normalized to yield a unit generalized mass matrix, namely

$$[GM_b] = [\chi_b]^T([GM_f] - [\phi_f]^T[M_f - \Delta M_b][\phi_f])[\chi_b] = [I] \tag{8}$$

which yields

$$[GK_b] = [\omega_b]^2 \tag{9}$$

The mode-shape matrix of the basic case is calculated by

$$[\phi_b] = [\phi_f][\chi_b] \tag{10}$$

The control mass-coupling matrix is transformed to the basic system by

$$[M_{c_b}] = [\chi_b]^T[M_{c_f}] + [\phi_b]^T[\Delta M_b][\phi_c] \tag{11}$$

where the second term is nonzero only when the difference between the nominal and the basic cases involve masses at the control surfaces. The tabulated GAF matrices are transformed by

$$\begin{aligned}[Q_{bb}(ik)] &= [\chi_b]^T[Q_{fb}(ik)][\chi_b] \\ [Q_{bc}(ik)Q_{bg}(ik)] &= [\chi_b]^T[Q_{fc}(ik)Q_{fg}(ik)]\end{aligned} \tag{12}$$

It should be noted that while $[\omega_f]$ and $[\phi_f]$ are not directly related to natural frequencies and modes of the real structure, most frequencies and modes in $[\omega_b]$ and $[\phi_b]$ are normally practically identical to those derived directly from the finite element model of the basic structure. The rest of the frequencies and modes in $[\omega_b]$ and $[\phi_b]$ contain the information introduced by the fictitious masses and must be included in the aeroelastic model for an accurate structural variation analysis.

Time-domain aeroelastic modeling requires the transformed tabulated GAF matrices of Eq. (12) to be approximated by rational interpolation functions in the s domain. The MS approximation function[7,8] is

$$\begin{aligned}[\bar{Q}_{bb}(\bar{s})\bar{Q}_{bc}(\bar{s})\bar{Q}_{bg}(\bar{s})] &= [Q_{bb}(0)Q_{bc}(0)Q_{bg}(0)] \\ &+ [A_{1_b}A_{1_c}A_{1_g}]\bar{s} + [A_{2_b}A_{2_c}0]\bar{s}^2 \\ &+ [D](\bar{s}[I] - [R])^{-1}[E_bE_cE_g]\bar{s}\end{aligned} \tag{13}$$

where $\bar{s} = sb/V$. The user defines the $m \times m$ $[R]$ and two approximation constraints (for each term) that cause the $[A_1]$ and $[A_2]$ matrices to be dependent variables. The $[D]$ and $[E]$ real coefficient matrices are calculated by an iterative nonlinear physically-weighted least-square procedure that fits the tabulated matrices of Eq. (12). The physical weighting algorithm[8,12] weights the tabulated data according to open-loop aeroelastic response characteristics at a selected dynamic pressure $q = q_d$. It has been shown that the resulting model is applicable to open- and closed-loop analyses with large dynamic pressure variations[8-10,12] and moderate structural variations.[2] The applicability of the physically weighted approximation to models with large local structural variations is demonstrated in the numerical example section.

A full description of the state-space aeroservoelastic model resulting from the MS approximation is given in Ref. 14. Once the model is constructed for the basic case, the only portion which is changed due to structural variations is the system matrix of the free equation of motion

$$\begin{Bmatrix}\dot{\xi} \\ \ddot{\xi} \\ \dot{x}_a\end{Bmatrix} = \begin{bmatrix}0 & [I] & 0 \\ -[\bar{M}]^{-1}[\bar{K}] & -[\bar{M}]^{-1}[\bar{B}] & -q[\bar{M}]^{-1}[D] \\ 0 & [E] & (V/b)[R]\end{bmatrix}\begin{Bmatrix}\xi \\ \dot{\xi} \\ x_a\end{Bmatrix} \tag{14}$$

where

$$[\bar{M}] = [GM_b] + \frac{qb^2}{V^2}[A_{2_b}]$$

$$[\bar{K}] = [GK_b] + q[Q_{bb}(0)]$$

$$[\bar{B}] = [GB_b] + \frac{qb}{V}[A_{1_b}]$$

The only matrix in Eq. (14) which has not been defined yet is $[GB_b]$. This matrix is usually not calculated from the finite element model, but assumed to be the diagonal matrix

$$[GB_b] = 2[\zeta_b][\omega_b] \tag{15}$$

where the diagonal structural $[\zeta_b]$ is either chosen using engineering judgment (typical values are 0.005–0.02) or measured in a ground vibration test. A root locus analysis of the system matrix of Eq. (14) with variable dynamic pressure yields the open-loop flutter q_F at which a branch crosses to the right side of the Laplace domain at $s = i\omega_F$. For closed-loop aeroservoelastic analysis, the state vector of Eq. (14) is augmented by control states and the loop is closed by relating the control inputs to sensor outputs.[14] The sensor output equations are based on modal deflection rows selected from $[\phi_b]$ of Eq. (10).

It should be noted that the formulation of Eq. (14) is not limited to the MS approximation method. Other approximation functions, like those of the term-by-term least-square, and the matrix Pade methods[13] can also be brought to the form of Eq. (13). The main difference is that the $[D]$ and $[E]$ matrices in these methods would be quite sparse and typically yield a considerably larger number of aerodynamic states.

Structural Variations

The aeroelastic free equation of motion for an actual case whose mass and stiffness matrices differ from those of the basic case by $[\Delta M_a]$ and $[\Delta K_a]$ is Eq. (14) with three modifications. The first two modifications are the replacements of $[GM_b]$ and $[GK_b]$ of Eqs. (8) and (9) by

$$[GM_{ba}] = [I] + [\phi_b]^T[\Delta M_a][\phi_b] \tag{16}$$

$$[GK_{ba}] = [\omega_b]^2 + [\phi_b]^T[\Delta K_a][\phi_b] \tag{17}$$

When the generalized damping matrix $[GB_b]$ of Eq. (14) is based on known damping characteristics of the structural elements (which is usually not the case), the first two modifications are sufficient. To evaluate the effect of these modifications on the damping characteristics, we inspect the $q = 0$ free equation of motion resulting from the second row of Eq. (14) with Eqs. (16) and (17)

$$[GM_{ba}]\{\ddot{\xi}\} + [GB_b]\{\dot{\xi}\} + [GK_{ba}]\{\xi\} = \{0\} \tag{18}$$

The eigensolution resulting from Eq. (18) with $[GB_b] = 0$ yields the natural frequencies $[\omega_a]$ and the associated eigenvectors $[\chi_a]$, normalized to unit generalized mass, which yields

$$[\chi_a]^T[GM_{ba}][\chi_a] = [I] \tag{19}$$

It should be noted that the ω_a values are identical to those obtained from Eq. (6) for the same structural variation. A $[\chi_a]$ coordinate transformation of Eq. (18) yields diagonal mass and stiffness matrices, but a nondiagonal damping matrix

$$[GB_a] = [\chi_a]^T[GB_b][\chi_a] \tag{20}$$

If we want to obtain an effectively diagonal generalized damping matrix, we replace $[GB_b]$ by the nondiagonal matrix

$$[GB_{ba}] = 2[GM_{ba}][\chi_a][\zeta_a][\omega_a][\chi_a]^T[GM_{ba}] \tag{21}$$

which, when substituted in Eq. (20) instead of $[GB_b]$ using Eq. (19), yields

$$[GB_a] = 2[\zeta_a][\omega_a] \tag{22}$$

where $[\zeta_a]$ is the desired structural damping coefficient matrix.

Table 1 Natural frequencies and modes of the coupled and decoupled conditions

Coupled store connection		Decoupled store connection		
Mode no.	Frequency, Hz	Mode no.	Frequency, Hz	Description
1	0.000	1	0.000	Rigid body roll
2	7.023	3	7.083	First fuselage bending
3	7.856	4	8.907	First wing bending
4	13.069	2	5.249	Store pitch
5	16.161	5	16.110	Second fuselage bending
6	27.408	6	27.310	Second wing bending
7	38.271	7	35.980	First wing torsion
8	39.639	8	39.403	Store yaw
9	41.137	9	40.060	Fuselage torsion
10	49.922	10	49.853	Third fuselage bending

To summarize, the aeroelastic models associated with all the different structural variations are based on the same generalized coordinates as those of the basic case in Eq. (14). The eigenproblem associated with the undamped version of Eq. (18)

$$(-\omega^2[GM_{ba}] + [GK_{ba}])\{\xi\} = \{0\} \tag{23}$$

is first solved for $[\omega_a]$ and $[\chi_a]$ which satisfy Eq. (19). Equation (14) is then reconstructed with $[GM_{ba}]$ [Eq. (16)], $[GK_{ba}]$ [Eq. (17)], and $[GB_{ba}]$ [Eq. (21)]; replacing $[GM_b]$, $[GK_b]$, and $[GB_b]$, respectively. The use of a constant set of generalized coordinates results in efficient numerical procedures in the model construction phase, and in subsequent repetitive analyses such as structural optimization and time domain response with varying stiffness properties, which are beyond the scope of this article.

Numerical Example

Description of the Aeroelastic System

The purpose of the numerical example is to demonstrate that the proposed fictitious mass modeling method is useful, easy to apply, and yields accurate and efficient aeroservoelastic models. The aeroelastic system chosen for this purpose represents a realistic modern control-augmented flight vehicle. For the sake of clarity, we chose to analyze the effect of large variations of a single stiffness term which has a drastic effect on aeroelastic characteristics.

The numerical example deals with a modified finite element model of the active flexible wing (AFW) wind-tunnel model tested at NASA Langley Research Center. A top view of the NASTRAN finite element model is given in Fig. 1. A description of the aerodynamic model is given in Ref. 9. The tip store is connected to the wing through a decoupling mechanism designed to decouple the pitch motion of the store and that of the wing when flutter occurs. The mechanism is modeled by two grid points located at the store c.g., and rigidly interconnected in all directions except pitch. The pitch connection is through a rotational spring whose nominal "coupled" condition is with pitch stiffness of k_θ = 67,740 lb-in./rad. When the decoupling mechanism is activated, the spring changes to "decoupled" condition with k_θ = 2382 lb-in./rad (a 96.5% reduction). The store pitch moment of inertia about the connection point is 1.68 lb-in.-s.^{2}

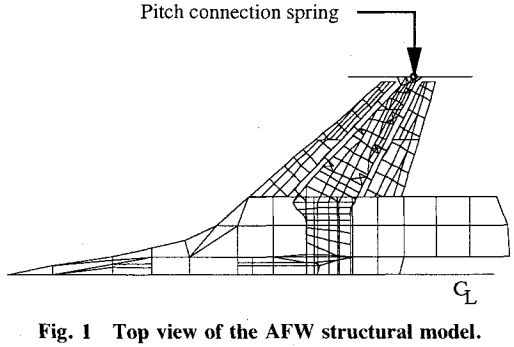

Fig. 1 Top view of the AFW structural model.

The 10 lowest antisymmetric natural frequencies of the coupled and decoupled conditions, and a description of the modes are given in Table 1. It can be observed that the main effect of the stiffness reduction is in reducing the frequency of the store pitch mode from 13.1 to 5.2 Hz. The pitch spring distortions in the decoupled model modes are generally considerably larger than those of the corresponding coupled model modes.

The ISAC code, a recent version of Ref. 15, was used to generate oscillatory aerodynamic force matrices for the 21 lowest frequency modes and 4 control surface modes, at 14k values between 0.0–1.5, using the doublet-lattice method at Mach 0.9. The STABCAR code[16] was used to obtain direct flutter results using the p-k method with equivalent structural damping values of $g = 2\zeta = 0.01$ for all the structural modes in both coupled and decoupled conditions. The flutter characteristics for the coupled case are q_F = 1.883 psi, ω_F = 11.87 Hz, and k_F = 0.269, and the main participants in the flutter mechanism are modes 3 and 4 of Table 1. The flutter characteristics for the decoupled case are q_F = 2.839 psi, ω_F = 30.80 Hz, and k_F = 0.698, and the main participants in the flutter mechanism are mode 6 and 7 of Table 1. It is clear that the stiffness change causes a drastic change in the flutter characteristics.

The four control surfaces are driven by third-order actuators. The control loop is closed by relating the actuator inputs to a single roll-rate sensor through a zero-order control law. The control gains were optimized in the numerical example of Ref. 2 to yield the required roll maneuverability with the best combination of flutter dynamic pressure and control robustness for the coupled case only. As will be shown later, the decoupled closed-loop flutter dynamic pressure with this control law is considerably lower than that of the coupled, which means that the decoupling mechanism would fail to suppress flutter with this control law.

Stiffness Variation Effects on Natural Frequencies

To demonstrate the necessity of the fictitious mass models, the calculations of decoupled natural frequencies from a coupled model, and vice versa, without using fictitious masses, are investigated first. A number of natural frequencies and mode shapes were calculated from the full finite element equation of motion, Eq. (1), of one case with $[M_f] = 0$. The stiffness difference between the two cases, $[\Delta K]$, and the modal deflections at the ends of the pitch spring were then used to calculate $[\phi_f]^T[\Delta K][\phi_f]$, and to construct the eigenproblem associated with Eq. (6) for the other case. The resulting natural frequencies were compared to those obtained directly from the finite element model. The effect of the number of coupled modes, used in calculating decoupled frequencies, on the resulting percentage errors of the lowest frequencies is shown in Fig. 2. The convergence is very slow, and it is clear that this is not a reasonable way to obtain a decoupled model. The effect of the number of decoupled modes used in cal-

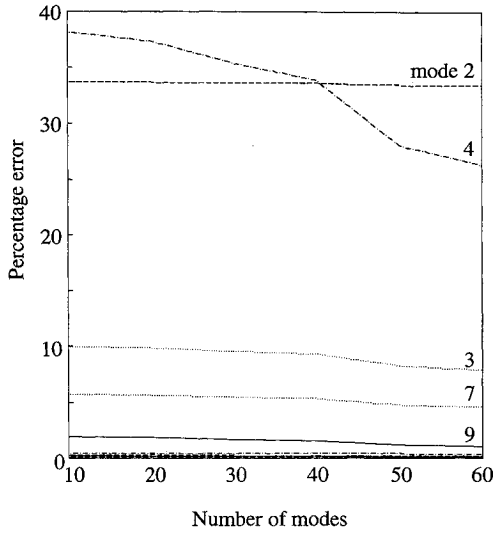

Fig. 2 Errors in decoupled frequencies calculated from coupled modes with no fictitious masses.

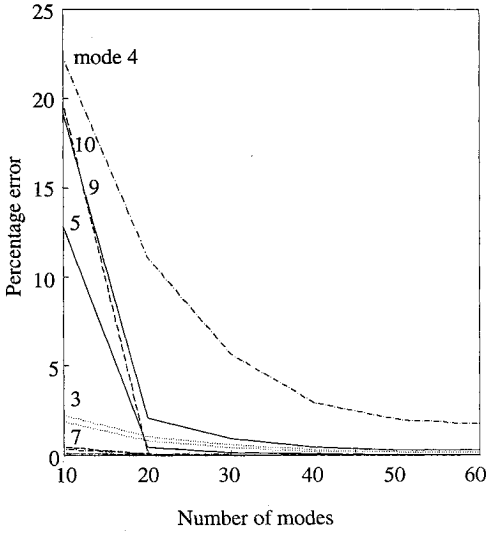

Fig. 3 Errors in coupled frequencies calculated from decoupled modes with no fictitious masses.

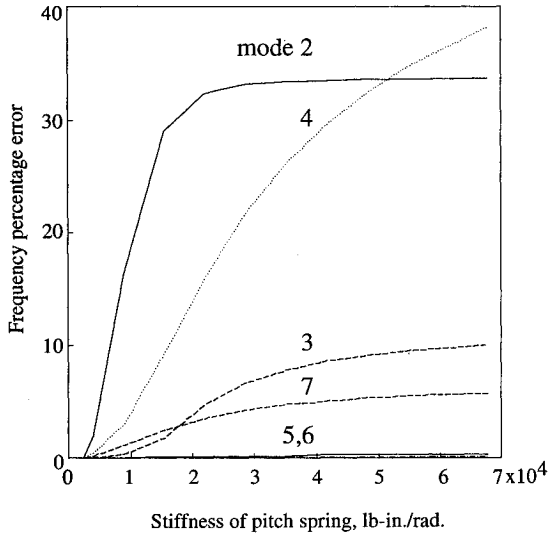

Fig. 4 Errors in decoupled frequencies calculated from model with various store pitch stiffness, no fictitious masses.

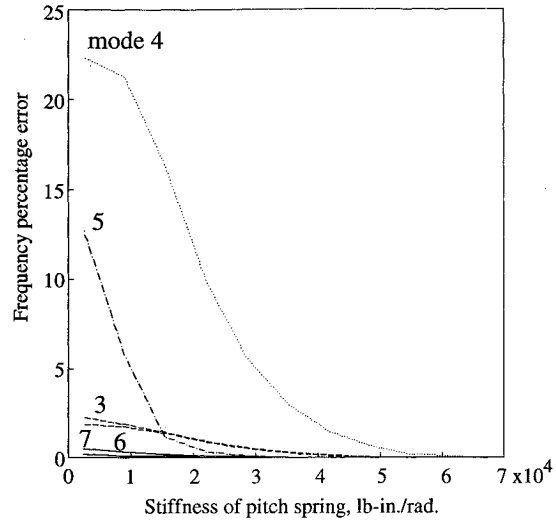

Fig. 5 Errors in coupled frequencies calculated from model with various store pitch stiffness, no fictitious masses.

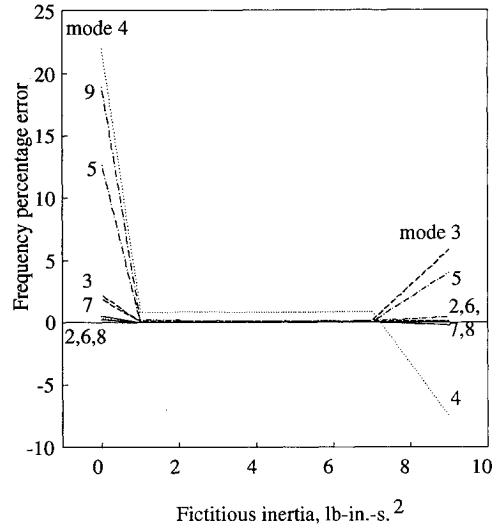

Fig. 6 Errors in coupled frequencies calculated from decoupled model with a fictitious mass.

culating coupled frequencies is shown in Fig. 3. The results are considerably better than those of Fig. 2, but the number of modes required for good accuracy of the important store pitch frequency is still quite large.

To investigate the effect of the magnitude of $[\Delta K]$, the coupled and decoupled frequencies were calculated from a model which is based on the 10 lowest frequency modes of a finite element model with an intermediate k_θ. The percentage errors of the resulting decoupled and coupled frequencies vs k_θ are shown in Figs. 4 and 5. It is clear from these figures, and from the trends in Figs. 2 and 3, that the simple ΔK approach (without fictitious masses) is totally unsuitable for large stiffness variation. It can also be deduced from the low stiffness range of Fig. 4 and from the high stiffness range of Fig. 5, that moderate stiffness changes between -40 to $+80\%$ can still be analyzed with the simple ΔK approach with frequency errors of less than 2%.

The decoupled model was chosen to form the nominal NASTRAN fictitious mass model for calculating the fictitious vibration modes $[\phi_f]$ from Eq. (1). A single fictitious pitch inertia was introduced at the wing end of the pitch spring. Ten fictitious modes ($n_f = 10$) were calculated and used to calculate the coupled frequencies by way of Eq. (6). The variation of the resulting percentage frequency errors with the magnitude of the fictitious inertia is shown in Fig. 6. The

Table 2 Coupled frequencies from decoupled model with fictitious mass

Direct coupled		Coupled frequencies from decoupled with fictitious masses				
Mode no.	Frequency, Hz	n_f = 5	8	11	14	Largest error, %
1	0.000	0.000	0.000	0.000	0.000	—
2	7.023	7.024	7.024	7.024	7.024	0.01
3	7.856	7.865	7.865	7.864	7.864	0.11
4	13.069	13.184	13.180	13.179	13.179	0.88
5	16.161	(122.56)	16.164	16.164	16.164	0.02
6	27.408		27.410	27.410	27.410	0.01
7	38.271		38.312	38.301	38.300	0.11
8	39.639		(139.04)	39.643	39.643	0.01
9	41.137			41.192	41.188	0.13
10	49.922			49.923	49.923	0.00
11	51.640			(160.28)	51.641	0.00
12	57.403				57.505	0.18
13	59.591				59.641	0.08
14	71.631				(185.72)	—

Table 3 Comparison between *p-k* and state-space flutter results

Pitch spring	Control loop	Flutter parameter	*p-k*		State-space	
			21 Modes	13 Modes	21 Modes	13 Modes
Coupled	Open	q_F, psi	1.883	1.889	1.878	1.884
		ω_F, Hz	11.87	11.88	11.88	11.89
	Closed	q_F, psi	1.924	1.921	1.943	1.940
		ω_F, Hz	8.672	8.663	8.710	8.701
Decoupled	Open	q_F, psi	2.839	2.958	2.832	2.948
		ω_F, Hz	30.80	30.88	30.69	30.78
	Closed	q_{F_1}, psi	0.791	0.795	0.797	0.801
		ω_{F_1}, Hz	5.074	5.071	5.073	5.070
		q_{F_2}, psi	3.193	3.279	3.122	3.207
		ω_{F_2}, Hz	29.44	29.63	29.34	29.51

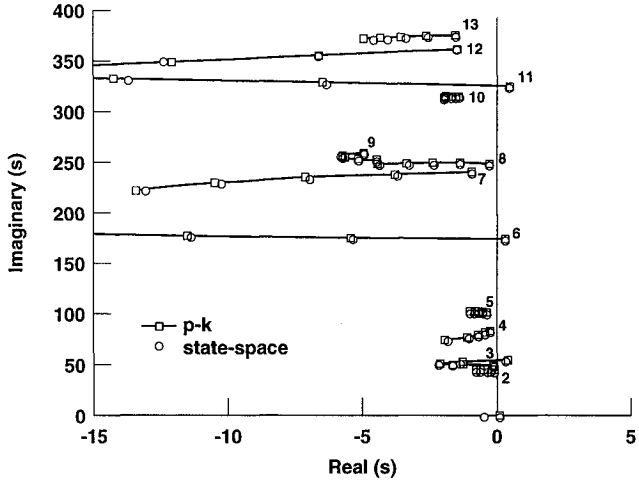

Fig. 7 Comparison of fictitious mass model roots with *p-k* roots, coupled pitch spring.

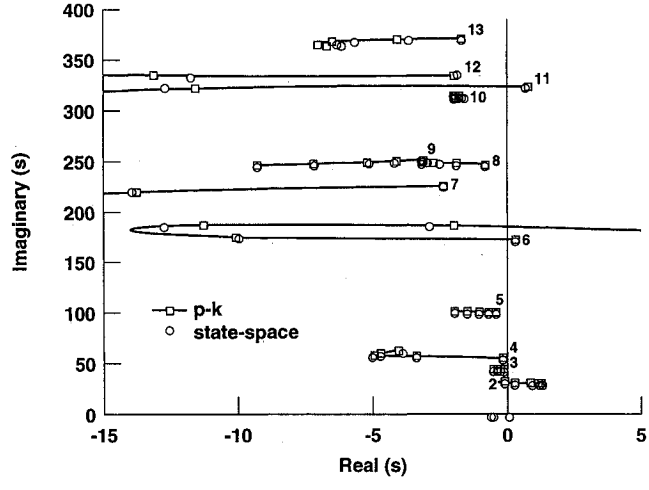

Fig. 8 Comparison of fictitious mass model roots with *p-k* roots, decoupled pitch spring.

errors for fictitious inertia between 1–7 lb-in.-s^2 (compared to 1.68 of the tip store) are insensitive to the magnitude of M_f, and are below 0.85%. This is a very significant improvement compared to the 22% error in the M_f = 0 case. The errors in the M_f = 9 lb-in.-s^2 case are due to ill conditioning caused by the large mass magnitude. The decoupled frequency errors obtained in the same way, but with ΔK = 0 are less than 0.6% (except for the ill-conditioned case). The results in Fig. 6 demonstrate that a proper choice of the values of the fictitious masses is easy and based on simple guidelines. On the one hand, the fictitious masses should be large compared to typical mass characteristics of the analyzed model (such as the total pitch moment of inertia of the tip store in our case). On the other hand, the fictitious mass values should not be large enough to cause numerical ill-conditioning. There is usually a very large gap between these lower and upper limits, as was also demonstrated in the modal substructuring applications of Ref. 5.

A comparison of coupled frequencies, obtained from n_f modes of the decoupled NASTRAN model with a single fictitious inertia of 3 lb-in.-s^2, with the directly calculated NASTRAN coupled frequencies, is given in Table 2. The highest frequency in each case is not a realistic one because it relates to local distortion introduced by the fictitious inertia. All the other frequencies in each case are very accurate and exhibit a negligible variation with n_f. The high accuracy of the frequencies also indicates that the associated mode shapes, $[\phi_b]$ of Eq. (10), are also accurate. The errors in obtaining decoupled frequencies from decoupled models with fictitious mass are smaller than those of the coupled frequencies.

Table 4 Comparison between direct and fictitious mass flutter results

Pitch spring	Control loop	Direct (13 modes) q_F, psi	Direct (13 modes) ω_F, Hz	Fictitious mass model (14 modes) q_F, psi	Fictitious mass model (14 modes) ω_F, Hz	q_F Error, %	ω_F Error, %
Coupled	Open	1.884	11.89	1.918	11.94	1.8	0.4
	Closed	1.940	8.701	1.946	8.694	0.3	−0.3
Decoupled	Open	2.948	30.78	3.077	30.94	4.4	0.5
	Closed	0.801	5.070	0.803	5.071	0.2	0.0
		3.207	29.51	3.375	29.71	5.2	0.7

Table 5 Comparison between decoupled roots of direct and fictitious mass models

Mode no.	Direct Re	Direct Im	Fictitious mass model With $[GB_{ba}]$ Re	Fictitious mass model With $[GB_{ba}]$ Im	Fictitious mass model With $[GB_b]$ Re	Fictitious mass model With $[GB_b]$ Im
1	−4.62	1.67	−4.59	1.71	−4.59	1.71
2	−0.47	30.10	−0.50	30.08	−0.78	30.06
3	−0.35	44.78	−0.35	44.77	−0.35	44.77
4	−2.71	57.52	−2.64	57.32	−2.68	57.34
5	−0.70	101.15	−0.69	101.16	−0.69	101.16
6	−6.23	190.87	−7.28	191.30	−7.37	191.21
7	−29.78	209.65	−28.49	209.55	−28.60	209.72

Direct State-Space Aeroelastic Models

Before evaluating the fictitious mass models, the MS modeling method was applied to the coupled and decoupled cases, separately. The modal structural data and the associated oscillatory generalized aerodynamic matrices used for the MS approximations and the state-space model constructions are identical to the data used for the respective STABCAR coupled and decoupled p-k solutions given previously. The MS approximations in all the cases in this work were performed using the MIST computer program,[8] with physical weighting of the aerodynamic data at $q_d = 1.5$ psi and with 2 weight peak-widening cycles.[12] The coefficients of the 21 × 21 $[\bar{Q}_{bb}]$ and the 21 × 4 $[\bar{Q}_{bc}]$ matrices of Eq. (13) were calculated with 8 aerodynamic lag roots (on the diagonal of $[R]$) of −0.1, −0.2, −0.35, −0.55, −0.8, −1.1, −1.5, and −2, which yields 8 aerodynamic states in Eq. (14). For closed-loop analysis Eq. (14) is augmented by 12 control system states representing the 4 third-order actuators.

The stability boundaries are found by a root-locus analysis with variable q. The state-space open- and closed-loop flutter results are compared to those of the p-k method in Table 3. It can be observed that the state-space results are in good agreement with those of the p-k method. The largest error is 2.3% in the second flutter dynamic pressure of the decoupled closed-loop case, which demonstrates that the MS approximation is valid for a wide range of q, and that 13 modes in each case are sufficient to predict flutter accurately. With a smaller number of modes, the flutter results start to change considerably (not shown).

Fictitious Mass State-Space Aeroelastic Model

A fictitious mass model which is based on a single set of modal coordinates and a single aerodynamic approximation is used in this subsection to calculate the stability boundaries of both coupled and decoupled cases. The baseline for comparisons are the separate 13 mode state-space results of Table 3. Since, as shown in Table 2, the fictitious mass model yields one nonrealistic natural frequency, the models below are based on 14 modes. It will be demonstrated that a fixed set of 14 modal coordinates can be used for high-accuracy open- and closed-loop stability analysis of the coupled and decoupled spring cases. This implies that any intermediate spring case can also be analyzed with the fixed modal coordinates. The analysis of more than one spring case with the same 14 modes is much more efficient than separate direct 13-mode analyses which require separate model construction efforts.

The decoupled fictitious modes that were used to generate the 14 mode case of Table 2, and the control surface modes, were used to generate the associated $[Q_{fb}(ik)]$ and $[Q_{fc}(ik)]$ aerodynamic matrices by ISAC. These matrices, along with the control mass coupling matrix and the sensor modal deflection matrix were then transformed to the basic coupled conditions by Eqs. (10–12). The MS approximation of the resulting $[Q_{bb}(ik)]$ and $[Q_{bc}(ik)]$ matrices was then performed and used to construct the coupled state-space open- and closed-loop systems. Decoupled models were obtained by the introduction of $[GK_{ba}]$ of Eq. (17) and $[GB_{ba}]$ of Eq. (21) to Eq. (14), instead of $[GK_b]$ and $[GB_b]$. The resulting flutter dynamic pressures and frequencies are compared in Table 4 to those obtained directly by separate state-space models. Because the physical weighting in the aerodynamic approximation of the fictitious mass model was performed with a coupled pitch spring, the decoupled errors are generally larger than the coupled ones, but still not larger than 5.2% in q_F and 0.7% in ω_F. The coupled and decoupled closed-loop root loci obtained from the fictitious mass models are compared in Figs. 7 and 8 to the direct 13-mode p-k roots. The dynamic pressure varies in the coupled case (Fig. 7) from 0 to 2 psi with symbols appearing every 0.5 psi, and in the decoupled case (Fig. 8) from 0 to 4 psi with symbols at every 1 psi. The mode numbers appear in the figure near the zero dynamic pressure points. The associated flutter conditions (where branches cross the imaginary axis from left to right) were given in Tables 3 and 4. It can be observed that the fictitious mass state-space models yield high accuracy results in the entire frequency range of interest and in a wide region off the imaginary axis.

To evaluate the effect of the damping modification suggested in Eq. (21), the decoupled open-loop characteristic roots of Eq. (14) associated with the 7 lowest frequency modes, at $q = 2$ psi are given in Table 5 for three cases, the direct 13-mode case, the fictitious mass case with $[GB_{ba}]$ replacing $[GB_b]$ (as done in creating Table 4), and the fictitious mass case without this replacement. We can see that the first two

cases agree quite well, and that the second real part in the last case (-0.78, which reflects the damping of the important store pitch mode) deviates by 66% from that of the direct case. Table 5 also demonstrates the accuracy of the proposed method in predicting subcritical characteristic roots over a wide range of stiffness variations.

Application of the fictitious-mass approach to cases with simultaneous large structural variations at different locations would require more fictitious masses. Consequently, more nonrealistic modes would have to be included, which decreases the model efficiency. The proposed method is still expected to be very efficient for a small number of large-variation locations, such as several external-store attachments or movable-surface actuators.

Conclusions

The standard procedures for the determination of aeroelastic models allow the investigation of some moderate stiffness variations by introducing stiffness coupling terms. Larger stiffness variations with these procedures require the costly regeneration of modal coordinates and the associated aerodynamic matrices. The presented fictitious mass method extends the allowable move limits in cases where large stiffness variations are expected at a small number of structural locations. An example, with a variable stiffness term which has a critical effect on aeroelastic characteristics, demonstrated that the introduction of one fictitious mass term near the variable stiffness extended the allowable move limits from -40%, $+80\%$ to more than -95%, $+2000\%$. The results are insensitive to the magnitude of the fictitious mass providing that it is large enough to cause significant local structural deformations in the low-frequency fictitious modes, and not large enough to cause numerical ill conditioning. The use of n_f fictitious modes yielded errors of less than 0.9% in the first $n_f - 1$ natural frequencies over the entire stiffness range. Only one application of the physically weighted minimum-state modeling procedure was required to adequately predict open- and closed-loop aeroelastic characteristics over large dynamic pressure and stiffness ranges of interest, with flutter dynamic pressure errors of less than 5.2%.

Acknowledgment

The work presented in this article was partially supported by NASA Grant NAGW-1708. This support is gratefully acknowledged.

References

[1]Bisplinghoff, R. L., and Ashley, H., *Principles of Aeroelasticity*, Wiley, New York, 1962, Chap. 9.

[2]Karpel, M., "Multidisciplinary Optimization of Aeroservoelastic Systems Using Reduced-Size Models," *Journal of Aircraft*, Vol. 29, No. 5, 1992, pp. 939–946.

[3]Hemmig, F. G., Venkayya, V. B., and Eastep, F. E., "Flutter Speed Degradation of Damaged, Optimized Flight Vehicles," *Journal of Aircraft*, Vol. 17, No. 12, 1980, pp. 833, 834.

[4]Karpel, M., and Newman, M., "Accelerated Convergence for Vibration Modes Using the Substructure Coupling Method and Fictitious Coupling Masses," *Israel Journal of Technology*, Vol. 13, Feb. 1975, pp. 55–62.

[5]Karpel, M., "Efficient Vibration Mode Analysis of Aircraft with Multiple External Store Configurations," *Journal of Aircraft*, Vol. 25, No. 8, 1988, pp. 747–751.

[6]Livne, E., "Accurate Calculation of Control Augmented Structural Eigenvalue Sensitivities Using Reduced Order Models," *AIAA Journal*, Vol. 27, No. 7, 1989, pp. 947–954.

[7]Karpel, M., "Design for Active Flutter Suppression and Gust Alleviation Using State-Space Aeroelastic Modeling," *Journal of Aircraft*, Vol. 19, No. 3, 1982, pp. 221–227.

[8]Karpel, M., "Time-Domain Aeroservoelastic Modeling Using Weighted Unsteady Aerodynamic Forces," *Journal of Guidance, Control and Dynamics*, Vol. 13, No. 1, 1990, pp. 30–37.

[9]Karpel, M., and Hoadley, S. T., "Physically Weighted Approximations of Unsteady Aerodynamic Forces Using the Minimum-State Method," NASA TP-3025, March 1991.

[10]Hoadley, S. T., and Karpel, M., "Application of Aeroservoelastic Modeling Using Minimum-State Unsteady Aerodynamic Approximations," *Journal of Guidance, Control and Dynamics*, Vol. 14, No. 11, 1991, pp. 1267–1276.

[11]Albano, E., and Rodden, W. P., "Double-Lattice Method for Calculating Lifting Disturbances of Oscillating Surfaces in Subsonic Flow," *AIAA Journal*, Vol. 2, No. 2, 1969, pp. 279–285.

[12]Karpel, M., "Extension to the Minimum-State Aeroelastic Modeling Method," *AIAA Journal*, Vol. 29, No. 11, 1991, pp. 2007–2009.

[13]Tiffany, S. H., and Adams, W. M., Jr., "Nonlinear Programming Extensions to Rotational Approximation Methods of Unsteady Aerodynamic Forces," NASA TP-2776, July 1988.

[14]Karpel, M., "Reduced-Order Aeroelastic Models via Dynamic Residualization," *Journal of Aircraft*, Vol. 27, No. 5, 1990, pp. 449–455.

[15]Peele, E. L., and Adams, W. M., "A Digital Program for Calculating the Interaction Between Flexible Structures, Unsteady Aerodynamic and Active Controls," NASA TM-80040, June 1979.

[16]Adams, W. M., Jr., Tiffany, S. H., Newsom, J. R., and Peele, E. L., "STABCAR—A Program for Finding Characteristic Roots of Systems Having Transcendental Stability Matrices," NASA TP-2165, June 1984.